PAPER

Check for updates

Revealing the flame retardancy of cotton fabrics treated with ammonium ethylenediamine tetramethylenephosphonate and trimethylol melamine†

Yong-Man Jang,*[a] Chol-Jin Kim,[a] Ju-Yong Kim,[a] Dae-Hyok Mun[a] and Chol-Jun Yu [ID] *[b]

Phosphorus-nitrogen containing polymers have been attracting considerable interest as potential flame retardants (FR) for cotton fabrics. In this work, we report an experimental-theoretical joint study on flame retardancy of cotton fibres treated with ammonium ethylenediamine tetramethylenephosphonate (**AEDTMP**) as FR and trimethylol melamine (**TMM**) as binder. Through material characterization and FR test, we find that the cotton fabric samples treated with 5% **AEDTMP** and 5% **TMM** solutions exhibit better flame retardancy and durability than those with 25% **AEDTMP** solution by forming multilayer coatings on the fabrics. Our calculations within the density functional theory framework reveal that the P–O–C and C–O–C bonds are newly formed by reactions between the **AEDTMP** FR and **TMM** binder, and the multilayer coating enhances such binding reactions. Our work highlights that the multilayer coating with **AEDTMP** of lower density is superior for flame retardancy and durability of treated cotton.

1 Introduction

During the past decades, flame retardants (FRs) have attracted significant interest in the textile industry to produce incombustible fabrics.[1–4] Numerous FRs have been developed for cotton fibres, which are widely used in clothing, household goods and industrial products but highly flammable.[5–11] Among them, phosphorus-containing compounds combined with nanophase substances, such as carbon nanotubes[12] and silicon-based nanoparticles,[13–17] have been found to notably reduce the flammability of cotton when coated on the cotton substrate. It has been revealed that the phosphorus-containing compounds form cross-linking structures on cotton fibres or react directly with cellulose by the help of binders or catalysts.[18,19] Although they may release formaldehyde, which is harmful to human health and the environment, the phosphorus-based FRs can effectively prevent the formation of combustible volatiles by affecting the pyrolysis while promoting the formation of char.[20] Up to now, many phosphorus-containing FRs have been developed for cotton fabrics, including phytic acid,[21–23] phosphorylated polymers,[24–27] vinylphosphonic acid,[28] biomolecules,[29,30] and organophosphorus polymers (known as Pyrovatex).[20]

The ammonium salt of ethylenediamine tetramethylene phosphonic acid (**AEDTMP**) was known as a non-toxic flame retardant with little environmental impact, since it does not contain toxic substances such as halogen and formaldehyde.[31] In **AEDTMP**, the phosphorus content is relatively high as being 23.1 weight (wt) percentage, which is higher than that in the natural phosphorus reservoir, ammonium phytate (21.8 wt%). The intumescent flame retardancy of cotton fabrics treated with **AEDTMP** can be enhanced owing to the synergistic effect of phosphorus and nitrogen. It was found that the functional groups of $-PO(O-NH_4^+)_2$ in **AEDTMP** might react with the hydroxyl groups $-OH^-$ of cellulose, resulting in formation of FR finishing of cotton fabrics.[31] Although several works have been reported for synthesis and characterization of **EDTMP**,[32–34] there is little paper for **AEDTMP**, except the work of Zheng *et al.* who reported the preparation of **AEDTMP** as an effective FR for cotton fabrics by using dicyandiamide as binder and shrinking agent.[31]

To fabricate the FR-treated cotton fibres, proper binder should be selected as it allows FRs to be firmly bonded to the cotton fibre. In fact, the chemical reactions between binder and FR and cotton fibre molecules occur to form chemical bonds between them, ensuring that no significant change is made in

[a]*Faculty of Chemistry, Kim Il Sung University, Ryongnam-Dong, Taesong District, Pyongyang, Democratic People's Republic of Korea. E-mail: ym.jang0816@ryongnamsan.edu.kp*

[b]*Faculty of Materials Science, Kim Il Sung University, Ryongnam-Dong, Taesong District, Pyongyang, Democratic People's Republic of Korea. E-mail: cj.yu@ryongnamsan.edu.kp*

† Electronic supplementary information (ESI) available: Tables for conformation search of **AEDTMP** and **TMM**, calculated FTIR wavenumbers, Fukui indices and durability test, and figures for molecular structures of **EDTMP** and **TMM**, HOMO−1 and LUMO+1, and EDX spectra. See DOI: https://doi.org/10.1039/d5ra00402k

the mechanical properties of cotton fabric. It was suggested that trimethylol melamine (**TMM**) can be a proper chemical binder for **AEDTMP**-treated FR cotton fabrics, demonstrating a little influence on the mechanical properties of cotton fabrics with a high anti-washing ability.[35,36] The hydroxyl groups of **TMM** was found to be chemically bonded with both the phosphonate group of **AEDTMP** and the hydroxyl groups of cellulose, leading to an enhancement of stable durability. In fact, the stable durability is one of the most important features of flame retardant fabrics, but it is contradictory to the flame retardancy; improving the durability by increasing the binder amount causes a decrease of the flame retardancy. To resolve such difficulty, one can use multilayer coatings, *i.e.*, alternating coatings of flame retardant and binder layers, being similar to the layer-by-layer (LBL) formation.[27,37–41]

In this work, we perform a combined experimental and theoretical work to reveal the flame retardancy of cotton fabrics treated with **AEDTMP** as flame retardant and **TMM** as binder. First-principles calculations within the density functional theory (DFT) framework are carried out to reveal the structures and reactivities of **AEDTMP** and **TMM** molecules and calculate the reaction energy between them. The three-steps reaction method is adopted to synthesize **AEDTMP** and the multilayer coating method is applied to fabricate the FR-treated cotton fabrics using the **AEDTMP**–**TMM** combined layer. Using nuclear magnetic resonance (NMR) spectroscopy, the structure of **AEDTMP** is verified in comparison with DFT calculation, and the flame retardancy of treated cotton fabrics are tested by using several characterization techniques.

2 Methods

2.1 Experimental method

Ethylenediamine, phosphorous acid, formaldehyde, melamine, ammonia solution and sodium carbonate were purchased from Aladdin Reagent (Shanghai, China). All chemicals were in analytical grade and used without further purification. **AEDTMP** was synthesized in the three steps as shown in Scheme 1; (1) ethylenediamine and formaldehyde were reacted to synthesize tetramethylol ethylenediamine (**TMED**), (2) **TMED** was reacted with phosphorous acid to make ethylenediamine tetramethylenephosphonic acid (**EDTMP**), and (3) **EDTMP** was neutralized with ammonia water, producing **AEDTMP**.

Firstly, ethylenediamine and distilled water were mixed into a solution using a motor stirrer. Then formaldehyde and sodium carbonate were added into the solution, while adjusting the pH as 8–9, and then the solution was stirred at 40 °C for 30 min to proceed the reaction, resulting in **TMED** solution. Next, the hydrochloric acid was added into the **TMED** solution, adjusting the pH as 1–2, and then a phosphorous acid solution of 0.4 M was added into the solution. The mixed solution was heated to 100–105 °C for 2 h, resulting in dark brown solution, and then cooled to room temperature. Ethanol solution was added, leaving overnight to get solid state **EDTMP**. The product of **EDTMP** was dissolved in water. The solution was stirred gently while dropping 20% aqueous ammonia solution, heated to 90–100 °C while refluxing for 1 h, and cooled to room
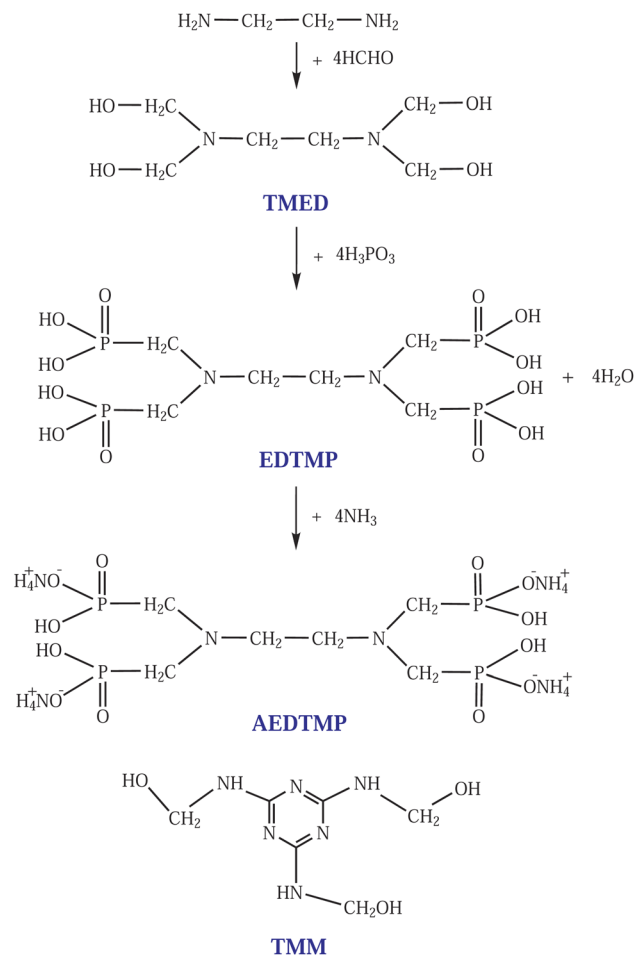
Scheme 1 Synthetic equations of tetramethylol ethylenediamine (**TMED**), ethylenediamine tetramethylene phosphonic acid (**EDTMP**) and ammonium salt of ethylenediamine tetramethylene phosphonic acid (**AEDTMP**). Chemical structure of trimethylol melamine (**TMM**) is also shown at the bottom.

temperature leaving overnight. By adding an ethanol solution, a solid state **AEDTMP** compound was precipitated. As a binder between **AEDTMP** and cotton fibre, **TMM** was prepared from melamine and formalin.

The molecular structures of the products were characterized by Fourier transform infrared (FTIR) analysis using the diamond-mounted Nicolet 6700 instrument. FTIR spectra were obtained at room temperature in the measurement wavenumber range of 400–4000 cm^{-1} with a resolution of 4 cm^{-1} and 64 scans using KBr compression method. The scanning electron microscopy (SEM) images of surface morphology were obtained with the JSM-IT200 instrument by using second-electron under an 5 kV accelerating voltage and 10 mm working distance. To characterized the compositions, energy dispersive X-ray (EDX) analysis was carried out. Thermogravimetric (TG) and derivative TG (DTG) curves were obtained using the Shimadzu TGA-50H instrument by heating the samples to 800 °C at a heating rate of 10 °C min^{-1}.

Cotton fabric ($\rho = 357$ g m^{-2}) was desized and washed. The fabric samples were immersed in 5% **AEDTMP** solution,

pressed at 5 kg cm^{-2} pressure, and moved at a speed of 2 m min^{-1}, resulting in 80% wet absorption. The FR-treated fabric samples were dried at 110 °C for 5 min, treated in a dip press with 5% **TMM** binder, and heated to 160 °C for 1 min. The samples were then neutralized with sodium carbonate solution, washed with 50 °C water for 30 min, and dried at 80 °C. This procedure was considered as one-time treatment. To realize the multilayer coating on the fabric samples, such treatment was repeated by 2, 3, 4 and 5 times. These samples were named 5FR-1, 5FR-2, 5FR-3, 5FR-4 and 5FR-5. By using 25% **AEDTMP** solution and 5% **TMM** solution, another fabric sample was prepared with one-time treatment, named 25FR-1 henceforth. Vertical flame tests were carried out according to the GB/T5455-1997 standard.[42] Accordingly, the cotton fabric samples with sizes of 30 × 8 cm were fired for 12 s, and the fire duration and damage length were measured. Limited oxygen index (LOI) values were measured using the HC-1 LOI instrument.

2.2 Computational method

DFT calculations were performed using the all-electron atomic orbital method as implemented in the NWChem (Version 7.2) package.[43] The 6-311++G(d,p) Gaussian-type basis functions were used as basis sets for all the elements. The hybrid B3LYP functional[44,45] was applied to treat the exchange–correlation interaction between the electrons. For the geometry optimizations of the molecules and molecular complex, the quasi-newton optimization method was applied using the DRIVER module with the default convergence criteria. Then, the frequency calculations were performed to determine the thermal correction (TC) and the zero-point correction (ZPC) to the total DFT energy, together with molecular vibrational frequencies. The basis set superposition error (BSSE) was corrected for binding energy calculations using the counterpoise method.[46]

3 Result and discussion

3.1 Molecular structures of AEDTMP and TMM

For a start, we considered the molecular structures of **AEDTMP** and **TMM** molecules under study in this work. Preliminarily, searching the conformational space of the molecules was conducted in order to derive conformers with the lowest energies, using the Conformers module of Materials Studio 2023. For this aim, the stochastic method based on random sampling, where the starting conformation was perturbed by randomly changing the values of all the variable torsion angles, was adopted with the use of COMPASS III (1.2) force field.[47] Since the ammonium cations are bound through the weak hydrogen bonds, we considered **EDTMP** in the conformation search rather than **AEDTMP**. The numbers of variable torsion angles were 11 and 6 for **EDTMP** and **TMM**, respectively. By setting the maximum number of conformers as 10 000, the numbers of the accepted conformers were found to be 7 and 1 for **EDTMP** (Table S1 and Fig. S1, ESI†) and **TMM** (Table S2 and Fig. S2, ESI†) molecules, respectively. Using the accepted conformers with the lowest energies as the initial structures, we performed geometry

optimizations of these molecules. Fig. 1 shows the optimized molecular structures of **AEDTMP** and **TMM**. The bond lengths, bond angles and torsion angles of the optimized molecules are listed in Table 1. It is clear from Fig. 1 that the ammonium NH_4^+ cations have been bonded to oxygen atoms of **EDTMP**$^-$ through hydrogen bonding of $NH_2–H_2\cdots O_2–POH–$ with average $O\cdots H$ bond distance of 1.561 Å. Though the hydrogen bonding, the ammonium cations should be strongly bound to **EDTMP** through the two $O\cdots H$ hydrogen bonds. With consideration of BSSE correction, TC and ZPC, the binding energy between the ammonium and **EDTMP** groups was calculated to be ~539.00 kcal mol^{-1}. The dipole moment was calculated to be 5.452 Debye. Within the **EDTMP** group, there are also several $O\cdots H$ hydrogen bonds between the adjacent PO_3H groups. In the PO_3H group, the bond length between P and O bonded with H ($P–O_H$ = 1.646 Å) was found to be shorter than that between P and O hydrogen-bonded with H of NH_4 ($P–O_{\cdots H}$ = 1.753 Å). Likewise, the N–H bond length (1.018 Å) was shorter than that between N and H hydrogen-bonded with O ($N–H_{\cdots O}$ = 1.110 Å). The most important torsion angle between N1–C1–C2–N2 was found to be 145.31°. For the case of **TMM** molecule, the dipole moment was calculated to be 1.134 Debye. The N–C bond length (1.359 Å) was found to be shorter than that between N and C
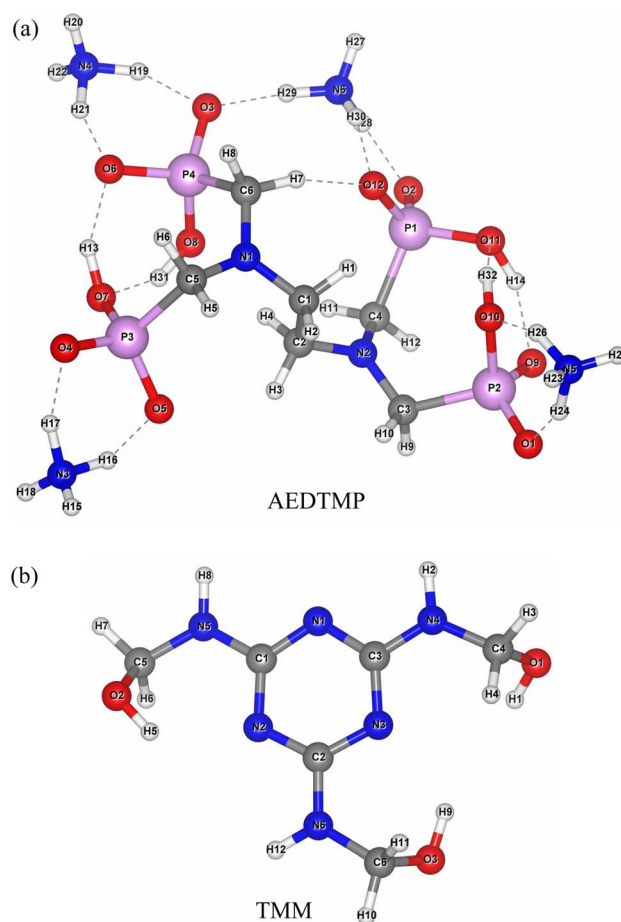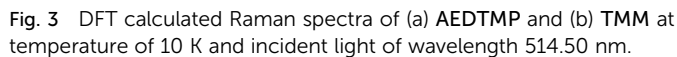

Fig. 1 Optimized molecular structures of (a) AEDTMP molecule and (b) TMM molecule.

© 2025 The Author(s). Published by the Royal Society of Chemistry

Table 1 Average bond lengths, average bond angles and torsion angles in ammonium salt of ethylenediamine tetramethylene phosphonic acid (AEDTMP) and trimethylol melamine (TMM) molecules optimized with B3LYP/6-311++G(d,p) method

Bond length (Å)		Bond angle (deg)		Torsion angle (deg)	
AEDTMP					
P–O$_H$	1.6462	O–P–O	108.192	N1–C1–C2–N2	145.308
P–O···$_H$	1.7533	P–C–N	116.079	C5–N1–C1–C2	92.898
P–C	1.9230	O–P–C	109.511	C3–N2–C2–C1	89.764
C–N	1.4492	C–N–C	119.683	P2–C3–N2–C2	129.139
C–C	1.5540	N–C–C	114.489	P1–C4–N2–C2	85.131
O–H	1.0116			P3–C5–N1–C1	80.141
C–H	1.0955			P4–C6–N1–C1	106.367
O···H	1.5607			O2–P1–C4–N2	169.954
N–H	1.0181			O1–P2–C3–N2	154.538
N–H···O	1.1099			O4–P3–C5–N1	172.145
				O3–P4–C6–N1	161.864
TMM					
N–C$_O$	1.4537	O–C–N	113.811	C4–N4–C3–N1	177.066
N–C	1.3591	C–N–C	122.721	O1–C4–N4–C3	89.594
C–O	1.4431	C–N–C$_r$	114.877	C5–N5–C1–N1	179.372
C–H	1.0914	N–C–N$_r$	117.464	O2–C5–N5–C1	63.507
N–H	1.0092	N$_r$–C–N$_r$	125.069	C6–N6–C2–N2	178.279
O–H	0.9817			O3–C6–N6–C2	64.615

bonded with O (N–C$_O$ = 1.454 Å). The average bond angle of C–N–C (122.72°) was larger than that of C–N–C$_r$ (114.88°), where C$_r$ is the carbon atom of the triazine ring. Meanwhile, the bond angle of N–C–N$_r$ (117.46°) was smaller than that of N$_r$–C–N$_r$ (125.07°), where N$_r$ is the nitrogen atom of the triazine ring. The structures of **AEDTMP** and **TMM** were confirmed by FTIR, as shown in Fig. 2 (see Table S3† for DFT calculated FTIR data). For the case of **AEDTMP**, several peaks were found to prove the molecular vibrations as decreasing the wavenumber. The wide and strong peaks at 3418 and 3123 cm^{-1} belong to the vibration of –OH and –NH groups. The asymmetric and symmetric

Fig. 2 FTIR spectra of (a) AEDTMP and (b) TMM measured from experiment.

Fig. 3 DFT calculated Raman spectra of (a) AEDTMP and (b) TMM at temperature of 10 K and incident light of wavelength 514.50 nm.

stretching vibration of CH$_2$ group are found at 2918 and 2846 cm^{-1}, and the O–H stretching vibration in the P–OH bond is found at 2719 cm^{-1}. Also, one can see the bending vibration of the O–H bond at 1631 cm^{-1}, the bending vibration of CH$_2$ at 1458 cm^{-1}, the N–H symmetrical bending vibration of NH$_4^+$ group at 1408 cm^{-1}, the stretching vibrations of P–O in the P=O and P–OH bonds at 1292, 1249, 1013 and 972 cm^{-1}, the stretching vibration of the P–C bond at 872 and 809 cm^{-1}, and the bending vibration of the P–O bond at 656 and 551 cm^{-1}. These molecular vibration modes are overall consistent with the previous work,[31] indicating that the final product is the **AEDTMP** molecule. For the case of **TMM**, the typical absorption bands of **TMM** were found, including the stretching vibration of the imino group (–NH–) at 3320 cm^{-1}, hydroxyl group (–OH) at 2923 cm^{-1}, methylene group (–CH$_2$–) at 1550 and 1488 cm^{-1}, and triazine ring at 961 and 810 cm^{-1} in almost consistent with the previous work.[48] Fig. 3 shows the Raman spectra of **AEDTMP** and **TMM** molecules calculated within DFT framework at temperature of 10 K and incident light with wavelength 514.50 nm. For the case of **AEDTMP**, some intense bands are observed at 233 cm^{-1} assigned to the C–C–N bending, 559 cm^{-1}, 2470 cm^{-1} for the P–H stretching, 3510–3610 cm^{-1} for the O–H stretching vibrations. For **TMM**, one can find an intense band at 617 cm^{-1} assigned to total symmetric stretching vibration of the ring, the band at 950 cm^{-1} for the CNC + NCN bending vibration, the bands at 3010–3140 cm^{-1} for the N–H stretching, and the band at 3650 cm^{-1} for the O–H stretching vibrations.

3.2 Frontier molecular orbitals and reactivity analysis

The chemical stability and reactivity of molecule can be estimated by calculating the frontier molecular orbital (FMO) levels, including the highest occupied molecular orbital (HOMO) and the lowest unoccupied molecular orbital (LUMO). Fig. 4 shows the calculated HOMO and LUMO with their energy levels of **AEDTMP** and **TMM** molecules (see Fig. S3 for
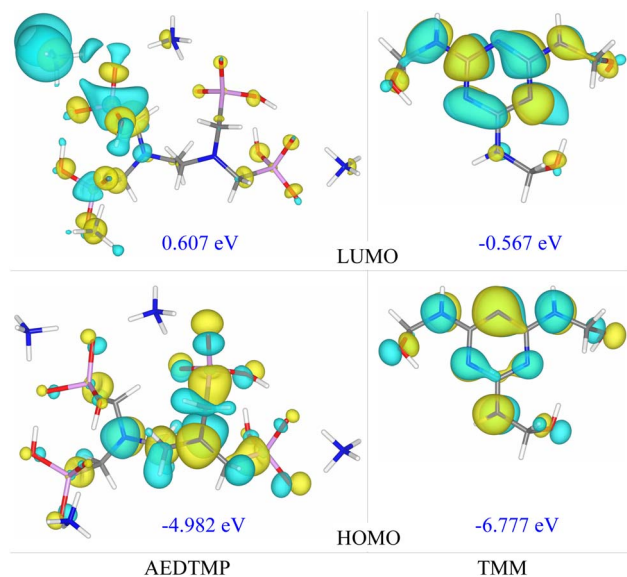
Fig. 4 Frontier molecular orbitals including the highest occupied molecular orbital (HOMO) and the lowest unoccupied molecular orbital (LUMO) of **AEDTMP** and **TMM** molecules.
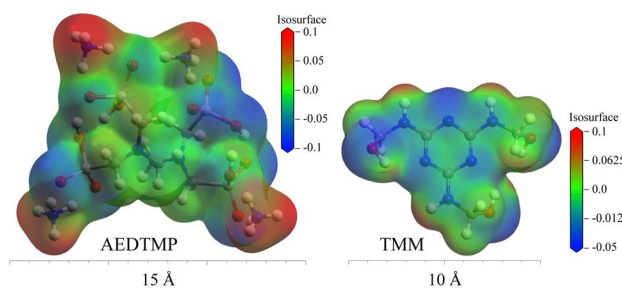

Fig. 5 Isosurface view of molecular electrostatic potential mapped onto total electron density at the value of 0.2|e| Å^{-3}.

HOMO−1 and LUMO+1, ESI†). The LUMO–HOMO energy gaps were found to be 5.589 and 6.210 eV for **AEDTMP** and **TMM** molecules, respectively, and might be assigned to the $\pi \rightarrow \pi^*$ transition nature. These gaps are relatively high, indicating that these molecules are quite chemically stable. The LUMO+1–HOMO−1 energy gaps were found to be 6.364 and 6.448, respectively. Based on the HOMO and LUMO energy values, we calculated the global chemical reactivity indexes of molecules, including chemical potential μ, electronegativity χ, hardness η, softness ζ, and electrophilicity index ω. When defining the ionization potential as $I = -E_{HOMO}$ and the electron affinity $A = -E_{LUMO}$, these are calculated as follows, $\mu = -(I + A)/2$, $\chi = (I + A)/2$, $\eta = (I - A)/2$, $\zeta = 1/(2\eta)$, and $\omega = \chi^2/2\eta$. Note that the μ value is the negative of the χ value, and the ω value represents the energy stabilization of molecule induced by maximal

electron flow from the environment.[49] Table 2 lists the corresponding quantities for **AEDTMP** and **TMM** molecules. It was found that the **AEDTMP** molecule has the lower hardness (2.795 eV), higher softness (0.179 eV^{-1}), and lower electrophilicity (0.856 eV) than the **TMM** molecule (3.105 eV, 0.161 eV^{-1}, and 2.171 eV), indicating that the former is softer and less reactive than the latter. As an effective interpretive tool for intermolecular interactions, we calculated the molecular electrostatic potential (ESP) mapped onto the isosurface of total electron density. Fig. 5 shows the calculated ESP isosurface view mapped onto the total electron density at the value of 0.2|e| Å^{-3} for **AEDTMP** and **TMM** molecules. The calculated ESP for **AEDTMP** indicated the regions with positive potentials (red colour) over the hydrogens of four NH$_4$ ammonium groups, while the regions with negative potentials (blue colour) over oxygens of phosphonic acid PO$_3$H group. For the case of **TMM**, the calculated ESP maps indicates the regions with positive potentials over hydrogens of NH and OH, whereas the negative potentials are located over the oxygen and nitrogen atoms. Therefore, the
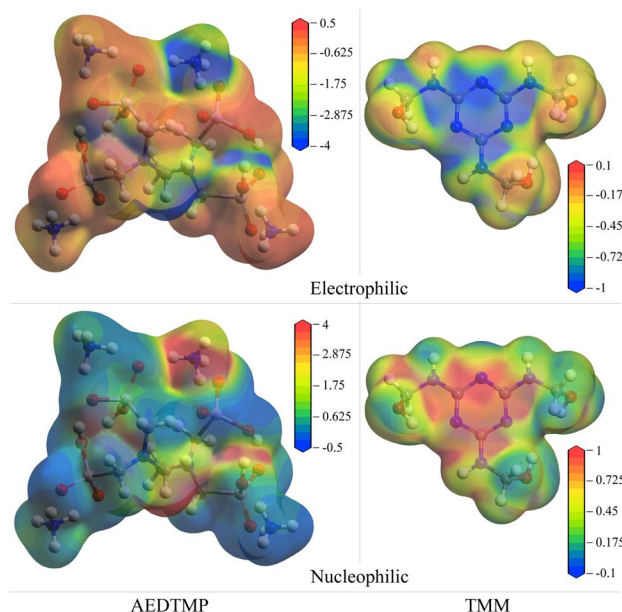
Table 2 HOMO energy (E_{HOMO}), LUMO energy (E_{LUMO}), HOMO−1 energy (E_{HOMO-1}), LUMO+1 energy (E_{LUMO+1}), and their gaps, with the deriving reactivity quantities including chemical potential, electronegativity, global hardness, global softness and global electrophilicity index, and dipole moment of **AEDTMP** and **TMM** molecules

Function	AEDTMP	TMM
E_{HOMO} (eV)	−4.982	−6.777
E_{LUMO} (eV)	0.607	−0.567
$\Delta E_{LUMO–HOMO}$ gap (eV)	5.589	6.210
E_{HOMO-1} (eV)	−5.557	−6.933
E_{LUMO+1} (eV)	0.807	−0.485
$\Delta E_{LUMO+1–HOMO-1}$ gap (eV)	6.364	6.448
Chemical potential μ (eV)	−2.188	−3.672
Electronegativity χ (eV)	2.188	3.672
Global hardness η (eV)	2.795	3.105
Global softness ζ (eV^{-1})	0.179	0.161
Global electrophilicity index ω (eV)	0.856	2.171
Dipole moment (Debye)	5.452	1.134

Fig. 6 Isosurface view of Fukui functions describing the chemical reactivity to electrophilic and nucleophilic attacks mapped on total electron density at the value of 0.2|e| Å^{-3}.

Paper

reaction between **AEDTMP** and **TMM** may occur through the condensation reaction of $OH–PO_2– + OH–CH_2– \rightarrow –PO_2–O–CH_2– + H_2O$. In addition to the global descriptors of the reactivity of molecule, we calculated the Fukui functions as a local reactivity descriptor, being defined as the derivative of electron density regarding to the change in the number of electrons while keeping the positions of the nuclei unaltered. Fig. 6 shows the calculated Fukui functions for electrophilic (f^-) and nucleophilic (f^+) attacks mapped on total electron density at the value of $0.2|e|$ $\mathring{A}^{-3}$ (see Tables S4 and S5† for Fukui indices). It was found that the O atoms of phosphonic acid group and the N atoms have the negative values of $\Delta f = f^+ - f^-$ while the C atoms and most of H atoms have the positive values of Δf, indicating that the formers act as nucleophile donating a pair of electrons while the latters act as electrophile accepting a pair of electrons in both molecules.

3.3 Flame retardancy of treated cotton fabric samples

The flame retardancy of cotton fabric samples treated with multilayers of alternating flame retardant 5% **AEDTMP** and binder 5% **TMM** layers was tested as increasing the treating times. The treating times are responsible for the number of layers in the multilayer coating. Fig. 7 shows the char length formed by vertical flame test for the cotton fabric samples treated with different treating times. In Fig. 7, the char length was found to gradually decrease as increasing the number of treating times. Table 3 summarizes the testing results such as LOI values and char lengths for the treated cotton fabric samples with different treating times. The table also lists the
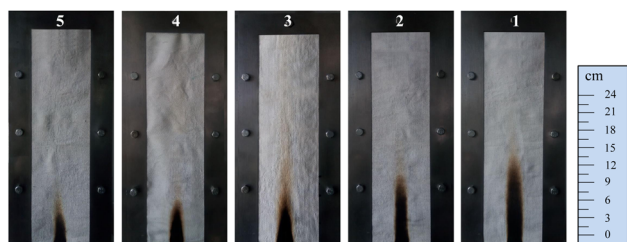

Fig. 7 Photos of cotton fabric samples treated with **AEDTMP** 5% and **TMM** 5% solutions after vertical flame test as increasing the number of treating times from 1 to 5.

Table 3 Testing results including LOI and char length for flame retardancy of cotton fabric samples, treated with 5% **AEDTMP** FR and 5% **TMM** binder solutions as increasing the treating times (5FR-*N*) and treated once with 25% **AEDTMP** FR solution (25FR-1)

Sample	**AEDTMP** portion	LOI (%)	Char length (cm)
5FR-1	8.6	26.2	13.5
5FR-2	11.2	29.5	11.2
5FR-3	14.4	32.1	9.1
5FR-4	17.9	37.5	8.6
5FR-5	21.5	42.4	6.2
25FR-1	21.5	42.6	5.9

AEDTMP portions in the treated samples. From the testing results, it was found that as increasing the number of treating times (*i.e.*, number of coating layers), the LOI value increased from 26.2% to 42.4% while the char length decreased from 13.5 cm to 6.2 cm, indicating the enhancement of flame retardancy as increasing the number of **AEDTMP–TMM** coating layers. This can be associated with the binding reaction rate; a relatively large amount of FR could be remained unreacted when one-time treating, but most amount of FR could be reacted with the binder when several times treating, thereby increasing the binding reaction rate. The multilayer coating leads to not only the FR-binder-cellulose chemical bond but also the FR-binder-FR chemical bond. That is, the binding reaction occurs more effectively for the multilayer coating, leading to stronger binding between **AEDTMP** flame retardant and cellulose. For the fabric sample treated with a denser 25% **AEDTMP** FR solution, the char length was found to be ~5.9 cm. This is even slightly shorter than that (~6.2 cm) of the 5 times-treated sample with 5% **AEDTMP** FR solution, indicating the improvement of flame retardancy with denser FR solution. However, it was found that the hand taste and colour of the single-treated sample with denser FR solution looked less than those with FR solution of lower density. After 20 times washing, all the samples presented increasing char lengths (Table S6, ESI†), indicating that their flame retardancy was deteriorated to some extent but was still kept within the flame retardancy standard. In fact, the 1FR-1 sample after 20 times washing lost
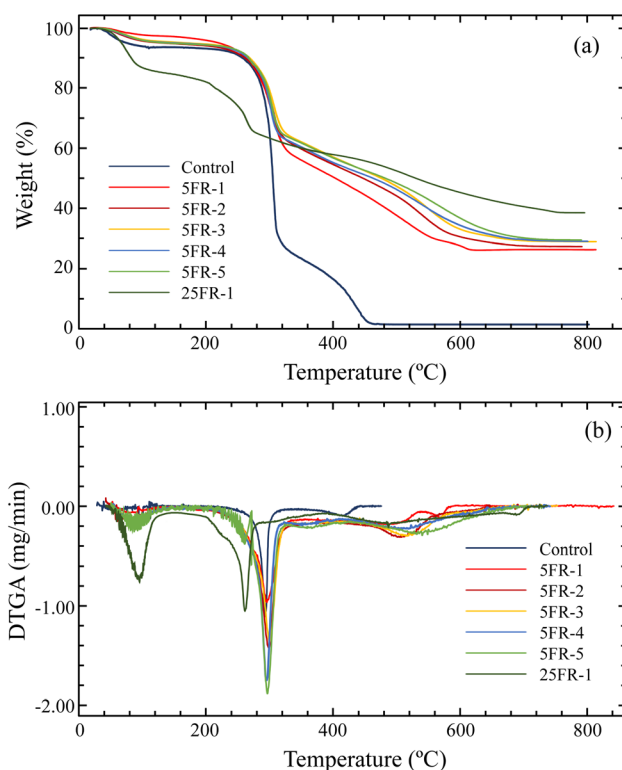

Fig. 8 (a) TGA and (b) DTGA curves of control, fabric samples treated with 5% **AEDTMP** FR solution and 5% **TMM** binder solution as increasing the treating times from 1 to 5, and the single-treated sample with 25% **AEDTMP** FR solution and 5% **TMM** binder solution.

its self-extinguishability in the vertical flame test and was burnt completely during about 23 s.

On the other hand, the 25FR-1 sample after 20 times washing presented the longer char length (11.1 cm) and the lower LOI value (26.5%) than those (8.9 cm and 34.6%) of the 5FR-5 sample. This indicates that the multilayer coating enhances the durability of treated cotton fabrics, as will be described more clearly through further TGA and SEM analysis. Fig. 8 shows the TG results of the control and flame retardant samples as increasing the number of treating times before washing within the temperature range of 30–800 °C. It was confirmed that the treated cotton samples exhibited the enhanced flame retardancy compared with the control, as the residue weights of the treated samples were found to be over 26% while the control had almost zero weight of residue at 800 °C. The cotton samples

treated with low density 5% **AEDTMP** FR solution, *i.e.* 5FR-*N* (*N* = 1 – 5) samples, exhibited the one-step decomposition in the temperature range of 300–305 °C with the residue weights of 26–30% at the end of the test. However, the single-treated sample with denser 25% **AEDTMP** FR solution, *i.e.* 25FR-1 sample, was found to be rapidly decomposed in two-step process at around 100 °C and 260 °C with 38% residue at 800 °C. For the case of 25FR-1 sample, the first-step decomposition at 100 °C is associated with the dehydration of the crystal water included in relatively large amount of nonbonded **AEDTMP**, while the second-step mass reduction at 260 °C is related with the decomposition of **AEDTMP** itself. For the cases of 5FR-*N* samples, there are barely crystal water because most of **AEDTMP** are bonded with cellulose or binder, leading to negligible mass reduction at around 100 °C. Moreover, most of
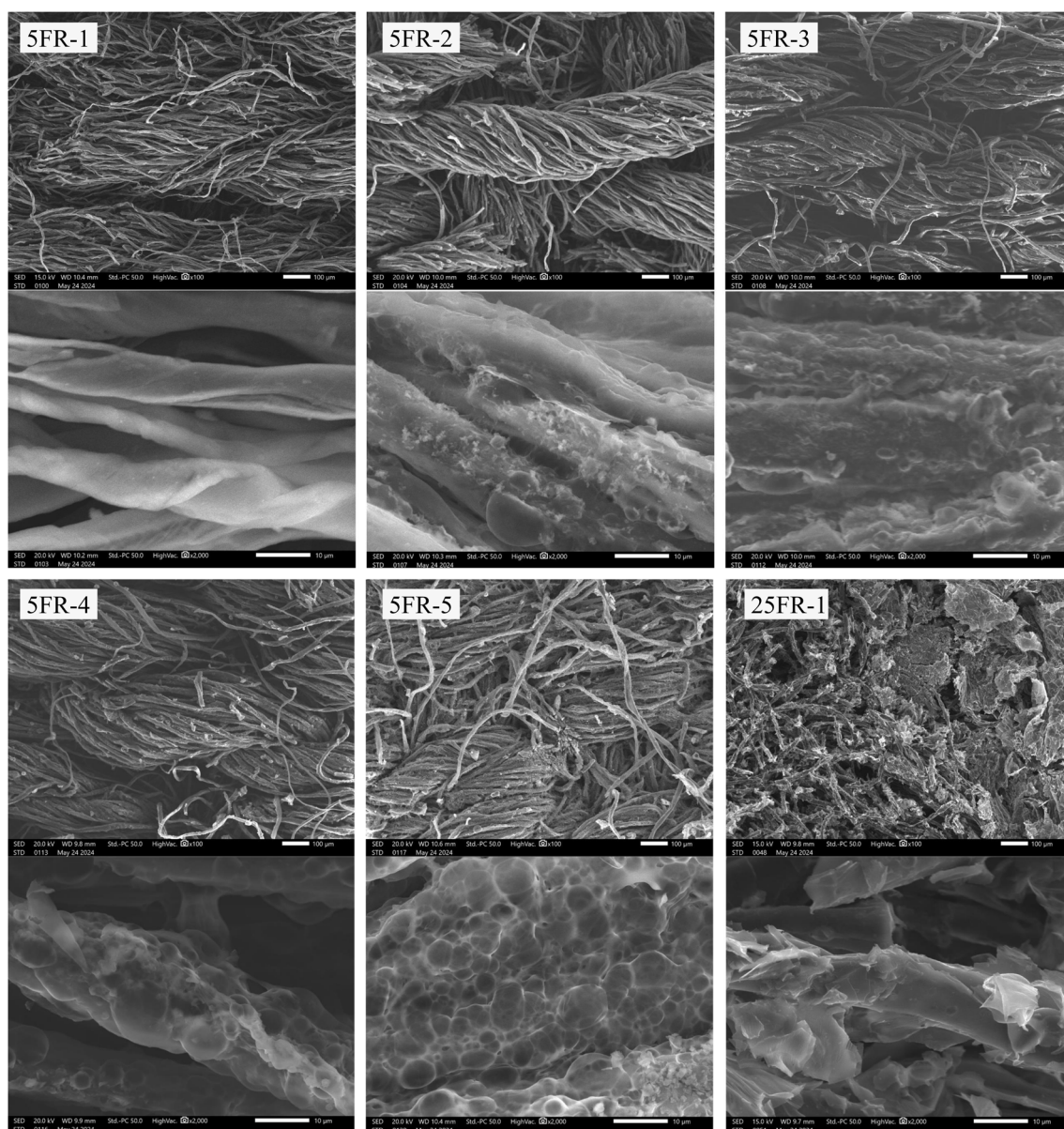

Fig. 9   SEM images of the cotton fabric samples treated with 5% AEDTMP FR solution and 5% TMM binder solution as increasing the treating times from 1 to 5 (5FR-*N*, *N* = 1 − 5) and the single-treated sample with 25% AEDTMP FR solution and 5% TMM binder solution (25FR-1).

mass reduction happened at higher temperature of 300 °C, being associated with that the binding reaction rate between FR-binder-cellulose became higher and thus most of **AEDTMP** were transformed to chemical substances with high thermal stability. The residue was found to be gradually increased from 26% to 30% as increasing the number of treating times from 1 to 5, indicating the enhancement of flame retardancy by multilayer coating. When compared with the higher dense FR-treated sample (25FR-1), the 5FR-*N* samples started the rapid decomposition at higher temperature (305 °C) and showed the smaller amount of residue (30%). This indicates that the higher dense FR-treated samples can exhibit higher degree of flame retardancy than the lower dense FR-treated samples.

To observe the char formation on cotton fibers after combustion, SEM images were analyzed for the samples treated with **AEDTMP** flame retardant and **TMM** binder with different treating times. Fig. 9 shows the SEM images with two scale magnifications of the treated samples with 5% **AEDTMP** FR solution as increasing number of treating times from 1 to 5 and the single-treated sample with denser 25% **AEDTMP** solution. It was found that the basic structure of cellulose in all the samples could be retained after combustion, and the amount of char formed by combustion increased as increasing the number of treating times. In particular, the intumescent char layer with a lump shape was formed on the surface of the single-treated sample with denser 25% FR solution, and the amount of char was larger than the 5 times-treated sample with lower 5% FR solution. Unlike the single-treated sample with 25% solution, however, one can see the uniform char layer containing lots of small-sized foam drops on the cellulose surface of the 5 times-treated sample with 5% solution. From this observation, it can be concluded that the mechanism of flame retardancy is associated with the intumescent P–N synergistic effect to form a porous char layer. In accordance with the above discussions, the single-treated sample with denser **AEDTMP** FR solution has superior flame retardancy.

In order to identify the elemental composition of char remaining in the flame retardant samples after combustion, the EDX analysis was carried out (see Fig. S4, ESI†). The contents of phosphorus and nitrogen elements on the surface of the char layer were found to increase in general as increasing the treating times, indicating the enhancement of P–N synergistic effect in the multilayer coating on the cotton fiber. When compared between the 5 times-treated sample with 5% FR solution and the single-treated sample with 25% FR solution, the phosphorus content of the latter sample (13.72 wt%) was found to be larger than that of the former sample (6.07 wt%), whereas the nitrogen content (11.24 wt%) was smaller than that of former sample (22.47 wt%). It should be noted that in the vertical flame test the char length of the single-treated sample with denser FR solution was measured to be shorter than that of the 5 times-treated sample with sparser FR solution, indicating that the phosphorus content is a crucial factor for enhancing the flame retardancy.

3.4 Discussion for FR and binder reaction

When the cotton fabric was treated with only **AEDTMP** FR solution, no durability was observed. This indicates that the coupling reaction barely occurs between the FR **AEDTMP** and cotton fiber. However, when adding the **TMM** binder solution and then conducting the heat treatment, significant durability was found, indicating that the **TMM** binder combines the cotton fiber with the FR **AEDTMP**. Moreover, the durability was found to be improved as increasing the treating times with the **AEDTMP** FR solution and **TMM** binder solution. This is related with the network-like cross-linking structure formed by the polycondensation reaction between the binder and flame retardant. This was confirmed by FTIR spectra of the flame-retardant samples.

As revealed by the reactivity analysis of molecules, the condensation reaction was suggested to occur between the –OH–PO_2 group of **AEDTMP** and the –OH–CH_2 group of **TMM**, producing a **AEDTMP–TMM** molecular complex and a water molecule. In this reaction, the resultant alkoxy group was bound to the P atom that is the nucleophilic reaction centre, leading to the formation of new P–O–C chemical bond. Fig. 10(a) shows the optimized structure of **AEDTMP–TMM** molecular complex. The two molecules were interconnected
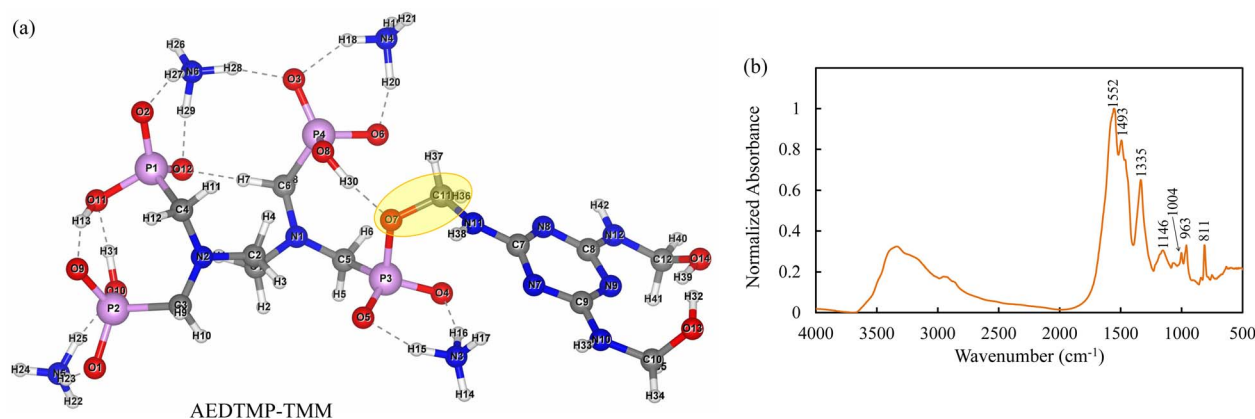

Fig. 10 (a) Optimized molecular structure of **AEDTMP–TMM** complex, where the semi-transparent yellow ellipse indicates the newly formed bond, and (b) its FTIR spectrum in the wavenumber rage of 4000–500 cm^{-1}.

Table 4 Characteristic absorption bands of reaction product between the AEDTMP flame retardant and the TMM binder and their assignments

Band (cm^{-1})	Vibration	Group
1552	NH in-plane bending	Secondary amine
1493	C=N cyclic	Melamine cycle
1335	C–N asymmetric stretching	Amine
1146	C–N symmetric stretching	Amine
1004	P–O stretching	Flame retardant
963	P–O–C stretching	Newly formed
811	NH out-of-plane bending	Secondary amine

through the bond PO$_2$–O–CH$_2$ with O–C bond length of 1.467 Å, P–O–C bond angle of 118.54° and N–C–O bond angle of 108.72°. Considering the TC and ZPC, the reaction energy was calculated to be 35.91 kcal mol^{-1}. To identify the chemical bonds newly formed by the condensation reaction, we measured the FTIR spectrum of the reaction product, **AEDTMP–TMM** complex, as shown in Fig. 10(b). Table 4 summarizes the characteristic absorption bands in the FTIR spectra of the reaction product, shown in Fig. 10(b). In the FTIR spectra of the reaction product, there are several characteristic bands originated from the **AEDTMP** flame retardant and the **TMM** binder, including 1552 and 811 cm^{-1} (NH in-plane and out-of-plane bending vibrations of the secondary amine), 1493 cm^{-1} (C=N cyclic vibration of the triazine ring), 1335 and 1146 cm^{-1} (C–N asymmetric and symmetric stretching vibrations of amine), and 1004 cm^{-1} (P–O stretching vibration of **AEDTMP**). Meanwhile, the absorption peak at the wavenumber of 963 cm^{-1} corresponds to the P–O–C stretching vibration of the newly formed group by the condensation reaction. The formation of this chemical bond may cause the shift of the absorption bands corresponding to the secondary amine to the lower wavenumbers of 1552 and 1335 cm^{-1}, compared to the absorption bands of 1563 and 1378 cm^{-1} corresponding to the secondary amine of **TMM**.

4 Conclusions

In this work, we investigated the enhancement mechanism of flame retardancy and durability of the cotton fabrics when treating with the phosphorus-rich flame retardant **AEDTMP** and binder **TMM** solutions by performing both experiment and first-principles calculations. The molecular structures of **AEDTMP** and **TMM** molecules were analyzed by measuring the optimized bond lengths, bond angles and torsion angles with DFT calculations, together with experimental FTIR and DFT-calculated Raman spectra. The reactivity analysis was performed by using the calculated HOMO, LUMO and their derivative quantities, and calculating the electrostatic potential and Fukui functions mapped onto the total electron density. The flame retardant cotton fabric samples were prepared by immerse-pressing fabrics in the 5% **AEDTMP** solution and 5% **TMM** binder solution as increasing treating times from 1 to 5 and the single-treated cotton sample was prepared by immersion in 25% **AEDTMP** solution. The vertical flame test was conducted to verify the flame retardancy and durability of the treated cotton

samples, revealing that the relevant properties were enhanced as increasing the treating times. Through the TG analysis, the 5 times-treated sample with 5% FR solution was found to commence the decomposition at lower temperature with larger char residue than the single-treated sample with denser 25% FR solution. The SEM images and EDX spectra showed significantly larger amount of char remaining on the cellulose surface, larger content of nitrogen element and smaller content of phosphorus element on the char surface of the 5 times-treated sample with sparser FR solution compared with the single-treated sample with denser FR solution. By performing optimization of **AEDTMP–TMM** complex and further FTIR analysis, it was confirmed that the chemical bonds of P–O–C and C–O–C were newly formed by reactions between the **AEDTMP** flame retardant and **TMM** binder. Overall, it was concluded that the multilayer coating with sparser **AEDTMP** FR solution is superior for durability of treated cotton.

Data availability

This data is available from the authors upon reasonable request.

Author contributions

Yong-Man Jang and Chol-Jun Yu developed the original project. Chol-Jin Kim, Ju-Yong Kim and Dae-Hyok Mun performed the experiments. Chol-Jun Yu carried out DFT calculations. Yong-Mang Jang drafted the first manuscript. Chol-Jun Yu supervised the work. All authors reviewed the manuscript.

Conflicts of interest

There are no conflicts to declare.

Acknowledgements

References

1 L. Taghi-Akbari, M. R. Naimi-Jamal, S. Ahmadi and S. Bakhtiyari, *Iran. Polym. J.*, 2024, **33**, 1129–1142.

2 M. S. Begum, A. Kader and R. Milašius, *Polymers*, 2023, **15**, 2563.

3 Y. Yang, X. Wang, X. Cheng, H. Li, X. Gu, J. Sun and S. Zhang, *Polym. Degrad. Stab.*, 2022, **200**, 109944.

4 J. Alongi and G. Malucelli, *RSC Adv.*, 2015, **5**, 24239–24263.

5 L. P. Delgado, A. P. Franco-Bacca, F. Cervantes-Alvarez, E. Ortiz-Vazquez, J. M. Ramon-Sierra, V. Rejon,

M. L. Aguirre-Macedo, J. J. Alvarado-Gil and G. Rodríguez-Gattorno, *Nanomaterials*, 2023, **13**, 463.

6 W.-C. Huang and H.-R. Chen, *Molecules*, 2023, **28**, 520.

7 A. M. Atta and H. M. Abomelka, *Mater. Chem. Phys.*, 2020, **260**, 124137.

8 D. Xu, S. Wang, Y. Wang, Y. Liu, C. Dong, Z. Jiang and P. Zhu, *Polymers*, 2020, **12**, 1538.

9 H. K. Nguyen, W. Sakai and C. Nguyen, *Materials*, 2020, **13**, 54.

10 L. J. Xu, W. Wang and D. Yu, *RSC Adv.*, 2017, **7**, 2044–2050.

11 F. Carosio and J. Alongi, *RSC Adv.*, 2015, **5**, 71482–71490.

12 X. Ding, F. Fang, T. Du, K. Zheng, L. Chen, X. Tian and X. Zhang, *Surf. Coat. Technol.*, 2016, **305**, 184–191.

13 C.-G. Choe, Y.-M. Jang, C.-H. Jo and C.-J. Yu, *Polym. Bull.*, 2023, **80**, 9727–9744.

14 H. Liu, S. Wang, J. Sun, X. Gu, H. Li and S. Zhang, *J. Mater. Sci.*, 2022, **57**, 2243–2256.

15 J. Liu, C. Dong, Z. Zhang, H. Sun, D. Kong and Z. Lu, *Cellulose*, 2020, **27**, 9027–9043.

16 J. Alongi, C. Colleoni, G. Rosace and G. Malucelli, *Polym. Degrad. Stab.*, 2014, **99**, 92–98.

17 J. Alongi and G. Malucelli, *Polym. Degrad. Stab.*, 2013, **98**, 1428–1438.

18 X. Zhou, X. Su, J. Zhao, Y. Liu, Y. Ren, Z. Xu and X. Liu, *Cellulose*, 2024, **31**, 3871–3892.

19 W. Lu, Z. Zeng, Z. He, Y. Liang, Y. Sun, S. Song, L. Wang and R. Liu, *J. Appl. Polym. Sci.*, 2022, **140**, 53546.

20 Z. Yang, X. Wang, D. Lei, B. Fei and J. H. Xin, *Polym. Degrad. Stab.*, 2012, **97**, 2467–2472.

21 O. Zilke, D. Plohl, K. Opwis, T. Mayer-Gall and J. S. Gutmann, *Polymers*, 2020, **12**, 1202.

22 M. Barbalini, M. Bartoli, A. Tagliaferro and G. Malucelli, *Polymers*, 2020, **12**, 811.

23 X. Zhao, Z. Liang, Y. Huang, Y. Hai, X. Zhong, S. Xiao and S. Jiang, *Prog. Org. Coat.*, 2021, **161**, 106453.

24 C.-H. Jo, Y.-M. Jang, D.-H. Mun, C.-J. Yu, C.-G. Choe and S.-G. Ri, *Polym. Degrad. Stab.*, 2023, **214**, 110366.

25 W.-G. Choe, W.-P. Kung, Y.-M. Jang, P. Choe, C.-G. Choe and C.-J. Yu, *Iran. Polym. J.*, 2024, **33**, 927–942.

26 Y.-M. Jang, C.-J. Yu, K.-S. Choe, C.-H. Choe and C.-H. Kim, *Cellulose*, 2021, **28**, 4455–4467.

27 H. F. Pan, W. Wang, Y. Pan, L. Song, Y. Hu and K. M. Liew, *Carbohydr. Polym.*, 2015, **115**, 516–524.

28 Z. Nooralian, M. P. Gashti and I. Ebrahimi, *RSC Adv.*, 2016, **6**, 23288–23299.

29 F. Bosco, A. Casale, C. Mollea, M. E. Terlizzi, G. Gribaudo, J. Alongi and G. Malucelli, *Surf. Coat. Technol.*, 2015, **272**, 86–95.

30 M. El-Shafei and A. A.-O. Elshemy, *Carbohydr. Polym.*, 2015, **118**, 83–90.

31 D. Zheng, J. Zhou, L. Zhong, F. Zhang and G. Zhang, *Cellulose*, 2016, **23**, 2211.

32 S. G. Mishra, D. K. Sawant, A. S. Chindarkar, A. N. Thamke, B. S. Kumar, A. C. Dey and M. S. Kulkani, *Appl. Radiat. Isot.*, 2022, **188**, 110386.

33 B. Guo, X. Lin, P. Liu, Y. Zeng and H. Fan, *Mater. Lett.*, 2019, **236**, 85–88.

34 N. Palta, B. V. Rao, S. N. Dubey and D. M. Puri, *Polyhedron*, 1984, **3**, 527–534.

35 K. M. Tang, C. Kan, J. Fan and S. Tso, *Cellulose*, 2017, **24**, 2619–2634.

36 C. Poon and C. Kan, *Carbohydr. Polym.*, 2015, **121**, 457–467.

37 L. Liu, Z. Huang, Y. Pan, X. Wang, L. Song and Y. Hu, *Cellulose*, 2018, **25**, 4791–4803.

38 Y. Jia, Y. Lu, G. Zhang, Y. Liang and F. Zhang, *J. Mater. Chem. A*, 2017, **5**, 9970–9981.

39 Y. Liu, Q.-Q. Wang, Z.-M. Jiang, C.-J. Zhang, Z.-F. Li, H.-Q. Chen and P. Zhu, *J. Anal. Appl. Pyrolysis*, 2018, **135**, 289–298.

40 Z.-F. Li, C.-J. Zhang, L. Cui, P. Zhu, C. Yan and Y. Liu, *J. Anal. Appl. Pyrolysis*, 2016, **126**, 216–223.

41 F. Carosio, A. D. Blasio, F. Cuttica, J. Alongi, A. Frache and G. Malucelli, *Ind. Eng. Chem. Res.*, 2013, **52**, 9544–9550.

42 L. Xu, W. Wang and D. Yu, *Carbohydr. Polym.*, 2017, **172**, 275–283.

43 E. Aprà, E. J. Bylaska, W. A. de Jong, N. Govind, K. Kowalski, T. P. Straatsma, M. Valiev, H. J. J. van Dam, Y. Alexeev, J. Anchell, *et al.*, *J. Chem. Phys.*, 2020, **152**, 184102.

44 C. Lee, W. Yang and R. G. Parr, *Phys. Rev. B*, 1988, **37**, 785–789.

45 A. D. Becke, *J. Chem. Phys.*, 1993, **98**, 5648–5652.

46 F. B. van Duijneveldt, J. G. C. M. Van Duijneveldt-Van De Rijdt and J. H. Van Lenthe, *Chem. Rev.*, 1994, **94**, 1873–1885.

47 R. L. C. Akkermans, N. A. Spenley and S. H. Robertson, *Mol. Simul.*, 2021, **47**, 540–551.

48 Y. Wu, Y. Li, L. Qin, F. Yang and D. Wu, *J. Mater. Chem. B*, 2013, **1**, 204–212.

49 Y.-K. Ri, S.-A. Kim, Y.-H. Kye, Y.-C. Jong, M.-S. Kang and C.-J. Yu, *RSC Adv.*, 2024, **14**, 16629–16638.